

Learning from tau appearance

P Migliozzi

I.N.F.N., Sezione di Napoli, Naples, Italy

F Terranova

I.N.F.N., Laboratori Nazionali di Frascati, Frascati (Rome), Italy

Abstract. The study of $\nu_\mu \rightarrow \nu_\tau$ oscillation and the explicit observation of the ν_τ through the identification of the final-state tau lepton (“direct appearance search”) represent the most straightforward test of the oscillation phenomenon. It is, nonetheless, the most challenging from the experimental point of view. In this paper we discuss the current empirical evidence for direct appearance of tau neutrinos at the atmospheric scale and the perspectives for the next few years, up to the completion of the CNGS physics programme. We investigate the relevance of this specific oscillation channel to gain insight into neutrino physics within the standard three-family framework. Finally, we discuss the opportunities offered by precision studies of $\nu_\mu \rightarrow \nu_\tau$ transitions in the occurrence of more exotic scenarios emerging from additional sterile neutrinos or non-standard interactions.

1. Introduction

The search for neutrino oscillations into flavors different from the initial one (“appearance”) has a decades-long history. Since 1998, however, the study of the $\nu_\mu \rightarrow \nu_\tau$ transition has played a unique role in the field of neutrino physics for a very special reason.

Neutrino oscillations [1] are a powerful tool to determine the squared mass differences of the rest masses of neutrinos because the oscillation phase is proportional to the ratio $(m_i^2 - m_j^2)L/E \equiv \Delta m_{ij}^2 L/E$. Here, i and j label the mass eigenstates ($i, j = 1, 2, 3$), L the source-to-detector distance (“baseline”) and E the neutrino energy. Oscillations also depend on the 3×3 matrix that describes the mismatch of flavor and mass eigenstates. It is the leptonic counterpart of the Cabibbo-Kobayashi-Maskawa matrix and is often referred to as the Pontecorvo-Maki-Nakagawa-Sakata (PMNS) matrix [2, 3]. This matrix can be parameterized by three angles, θ_{12}, θ_{23} and θ_{13} , and one CP-violating phase δ ‡. The experimental results obtained so far point to two very distinct mass differences, $\Delta m_{sol}^2 = \Delta m_{21}^2 \equiv m_2^2 - m_1^2 = 7.65_{-0.20}^{+0.23} \times 10^{-5}$ eV² [4] and $|\Delta m_{atm}^2| = |\Delta m_{32}^2| \equiv |m_3^2 - m_2^2| \simeq |m_3^2 - m_1^2| = 2.32_{-0.08}^{+0.12} \times 10^{-3}$ eV² [5]. Δm_{21}^2 is called the “solar mass scale” because it drives oscillation of solar neutrinos, but, of course, if the energy of the neutrino and the source-to-detector distance are properly tuned, it can be measured also employing man-made neutrinos, e.g., reactor neutrinos located about 100 km from the detector [6]. Similarly, atmospheric neutrinos mainly oscillate at a frequency that depends on Δm_{32}^2 (“atmospheric scale”). Accelerator neutrino experiments can see (actually, saw in K2K [7] and MINOS [8]) the same effect using neutrinos of energy $\mathcal{O}(1)$ GeV and baselines of a few hundreds of km.

Appearance has always been considered the most direct proof of the phenomenon of neutrino oscillation. Unfortunately, all sources that we have at our disposal to observe oscillations at the solar scale (solar and reactor neutrinos) produce ν_e (or $\bar{\nu}_e$) with energy well below the kinematic threshold for muon production. As a consequence, it is impossible to test in a straightforward manner the occurrence of $\nu_e \rightarrow \nu_\mu$ or $\nu_e \rightarrow \nu_\tau$ transitions through the observation of muons or taus produced by charged-current (CC) neutrino interactions with matter. At the atmospheric scale (atmospheric and multi-GeV artificial neutrinos from the decay in flight of pions), $\nu_\mu \rightarrow \nu_e$ transitions might be observed in appearance mode. Still, the peculiar structure of the leptonic mixing matrix suppresses this transition at least by one order of magnitude by virtue of the small θ_{13} angle [9, 10, 11]. Therefore, an appearance measurement that is aimed at observing a large (i.e. $\mathcal{O}(1)$) neutrino transition probability must resort to $\nu_\mu \rightarrow \nu_\tau$. In the current framework of interpretation of neutrino oscillation data - three active neutrinos non-trivially mixed by a 3×3 unitary matrix [12] - such probability is quite large for multi-GeV neutrinos at baselines of the order of 10^3 km. In this case, the oscillation probability is given by:

$$P(\nu_\mu \rightarrow \nu_\tau) \simeq \cos^4 \theta_{13} \sin^2 2\theta_{23} \sin^2 \Delta_{32} \quad (1)$$

‡ Additional Majorana phases cannot be observed by oscillation experiments [1].

$\Delta_{32} = \Delta m_{32}^2 L/4E$ being the oscillation phase (L is the baseline and E the neutrino energy in $c = \hbar = 1$ units) while θ_{13} and θ_{23} are the mixing angles of the third family with the first and second one, respectively. Due to the tri-bimaximal structure [13] of the mixing matrix ($\theta_{13} \simeq 0$ and $\theta_{23} \simeq \pi/4$), this probability is $\mathcal{O}(1)$ at the oscillation peak ($\Delta_{32} = \pi/2$).

Seeking for $\nu_\mu \rightarrow \nu_\tau$, i.e. observing final state ν_τ CC interactions, is a major experimental challenge. The source must produce neutrinos well above the kinematic threshold for tau production (3.5 GeV for scattering in nuclei). Moreover, the far detector has to be capable of selecting an enriched sample of tau leptons in the bulk of muons and hadrons produced by ν_μ CC and NC interactions. It comes as no surprise that the most direct test of the oscillation phenomenon through the observation of tau appearance still deserves a conclusive evidence. In 2010, however, important milestones have been achieved, especially by the SuperKamiokande and OPERA experiments. The aim of this paper is a careful examination of the present evidence for tau appearance as a direct probe of neutrino oscillations. In addition, we discuss what can be learned from $\nu_\mu \rightarrow \nu_\tau$ studies in the standard 3-family oscillation framework and in more exotic scenarios. We also anticipate the relevance of precision measurements of $\nu_\mu \rightarrow \nu_\tau$ to be performed by a future generation of short/long baseline experiments.

2. Past searches for tau appearance

At the beginning of the 90's, there were theoretical arguments [14, 15] suggesting that, in analogy with quark mixing, neutrino mixing angles should be small and that the heavier neutrino (mostly ν_τ) may have a mass of 1 eV, or larger, and therefore could be the main constituent of the dark matter in the universe. This hypothesis was based on two key assumptions:

- the interpretation of the solar neutrino deficit in terms of $\nu_e \rightarrow \nu_\mu$ oscillations amplified by matter effects, giving $\Delta m^2 \approx 10^{-5} \text{ eV}^2$;
- the input from see-saw mass-generation models [16], which predicts that neutrino masses are proportional to the square of the mass of the charged lepton, or of the 2/3 charge quark of the same family.

From these two assumptions one expects a $\nu_\mu \simeq \nu_2$ mass of $\sim 3 \times 10^{-3} \text{ eV}$ and a $\nu_\tau \simeq \nu_3$ mass of $\sim 1 \text{ eV}$, or higher.

The seeming concordance between cosmological and particle physics hints boosted enormously the search for tau appearance; in particular, it supported the design and construction of two high sensitivity short baseline experiments to discover $\nu_\mu \rightarrow \nu_\tau$ oscillations in the region of $\Delta m^2 \sim 10 \text{ eV}^2$. The two CERN experiments performing this search were NOMAD [17] and CHORUS [18], both exploiting the CERN SPS wide-band neutrino beam (WANF [19]) but with two quite different approaches.

2.1. The NOMAD experiment

The NOMAD experiment was designed to search for $\nu_\mu \rightarrow \nu_\tau$ in the WANF. The detector consisted of drift chambers used as target and tracking medium. They were optimized to fulfill two opposite requirements: a heavy target to collect as many interactions as possible and a light target to allow a precise tracking by reducing multiple scattering. In total there were 44 chambers with a fiducial mass of 2.7 tons and an active area of $2.6 \times 2.6 \text{ m}^2$. They were followed by a transition radiation detector (TRD) for e/π separation. Electron identification was performed with a pre-shower detector and a lead-glass electromagnetic calorimeter followed by an iron-scintillator sampling hadronic calorimeter, an iron absorber and a set of 10 muon chambers. The detector was located within a magnetic field of 0.4 T, perpendicular to the beam axis for momentum determination. In fact, the magnetic dipole hosting the NOMAD drift chambers was originally built for the UA1 experiment and it is currently used by the T2K Collaboration for the 280 m near detector [20].

The NOMAD experiment based its search for ν_τ on kinematical criteria. From the kinematical point of view, ν_τ CC events in NOMAD are fully characterized by the decay products of the primary τ . The spatial resolution of NOMAD did not allow the observation of a secondary vertex from τ decay. The presence of visible secondary τ decay products, τ_V , marks a difference with respect to NC interactions, whereas the emission of one (two) neutrino(s) in hadronic (leptonic) τ decays provides discrimination against ν_μ (ν_e) CC interactions (Fig. 1). Hence, in ν_τ CC events the transverse component of the total visible momentum and the variables describing the visible decay products have different absolute values and different correlations with the remaining hadronic system, H , than in ν_μ (ν_e) CC and NC interactions. The optimal separation between signal and background is achieved when all the degrees of freedom of the event kinematics (and their correlations) are exploited.

The maximum ν_τ signal allowed by limits from previous experiments [21, 22] was at least a factor of 0.0025 times smaller than the main ν_μ CC component and a rejection power against backgrounds of $\mathcal{O}(10^5)$ was required from the kinematic analysis. Therefore, the ν_τ appearance search in NOMAD was a kinematic-based search for rare events within a large background sample, as in Super-Kamiokande nowadays (see Sec.3). Similarly, in order to obtain reliable background estimates the Collaboration developed methods to correct Monte Carlo (MC) predictions with experimental data and defined appropriate control samples to check such predictions.

2.2. The CHORUS experiment

The approach followed by the CHORUS experiment was rather different. Instead of relying on a kinematic analysis, a detector based on nuclear emulsions with an ultra-high granularity ($1 \mu\text{m}$) was employed. A schematic picture of the CHORUS apparatus is shown in Fig. 2.

The *hybrid* setup was made of an emulsion target (800 kg), a scintillating

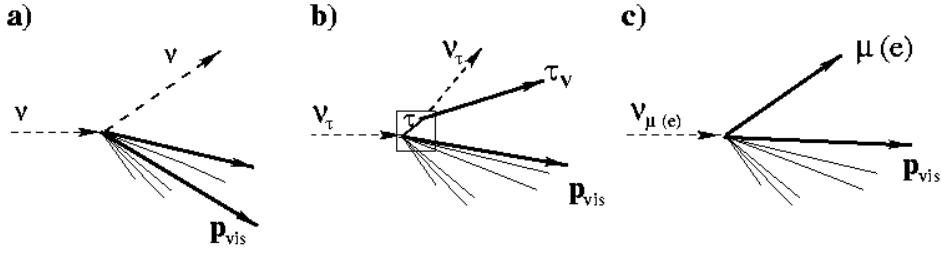


Figure 1. Signal and background topologies in NOMAD: a) NC background; b) ν_τ CC signal with subsequent τ decay; c) $\nu_\mu(\nu_e)$ CC background. The square indicates the reconstructed “primary” vertex for ν_τ CC interactions.

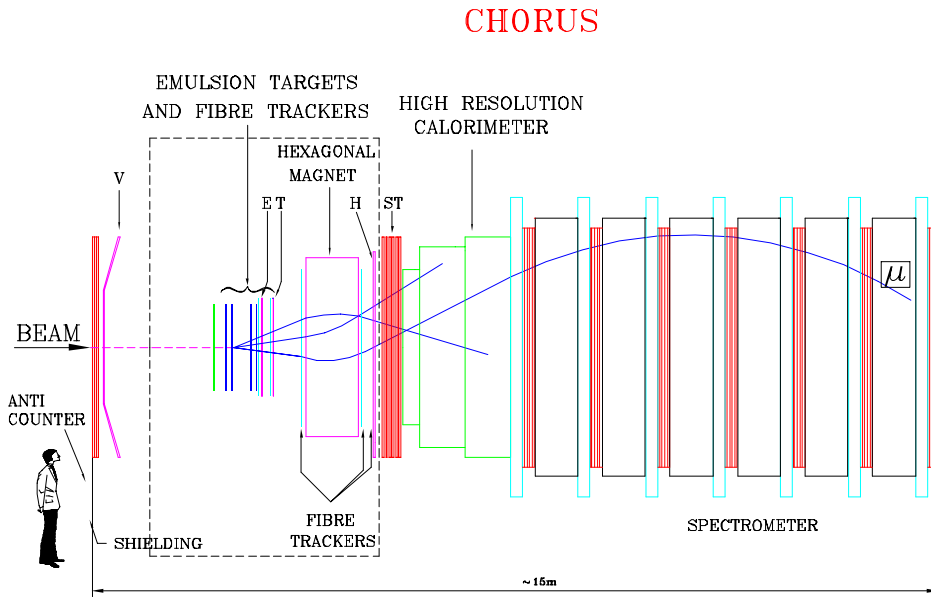


Figure 2. General layout of the CHORUS detector.

fibre tracker system, trigger hodoscopes, a magnetic spectrometer, a lead-scintillator calorimeter and a muon spectrometer.

The nuclear emulsions acted as the target and, simultaneously, as the detector of the interaction vertex and of the τ lepton decay [23]. The emulsions were subdivided in 4 stacks of 36 plates, oriented perpendicularly to the beam and with a surface of $1.44 \times 1.44 \text{ m}^2$. Each plate was made of a $90 \mu\text{m}$ transparent plastic film with $350 \mu\text{m}$ emulsion sheets on both sides.

The nuclear emulsion target was equipped with a high resolution tracker made of interface emulsions and scintillating fibre planes. Each stack was followed by three special interface emulsion sheets: two Changeable Sheets (CS), close to the fibre trackers, and a Special Sheet (SS), close to the emulsion stack. The sheets had a plastic base of $800 \mu\text{m}$ coated on both sides by $100 \mu\text{m}$ emulsion layers. Eight planes of target trackers of scintillating fibres ($500 \mu\text{m}$ diameter) [24], interleaved between the emulsion stacks, measured the trajectories of the charged particles with a precision of $150 \mu\text{m}$ in position

and 2 mrad in angle at the surface of the CS.

Downstream of the target region, a magnetic spectrometer was used to reconstruct the momentum and sign of charged particles. A hexagonal air-core magnet [25] produced a pulsed homogeneous field of 0.12 T. Field lines were parallel to the sides of the hexagon and the magnetized region extended for a depth of 75 cm in the direction of the beam. The tracking before and after the magnet was performed by a high resolution detector made of scintillating fibres (500 μm diameter) and complemented with a few planes of electronic detectors (streamer tube chambers in the 1994, 1995 and at the beginning of 1996 run, honeycomb chambers [26] afterward). The resulting momentum resolution $\Delta p/p$ was 30% at 5 GeV.

In addition to the detection elements described above and in order to perform a more precise kinematical analysis of the ν_τ decay candidates, the air-core hexagonal magnet region was equipped with large area emulsion trackers during the 1996 and 1997 runs.

A 100 ton lead-scintillating fibre calorimeter [27], together with a lead-scintillator calorimeter, followed the magnetic spectrometer and measured the energy and direction of electromagnetic and hadronic showers, together with a lead-scintillator calorimeter.

A muon spectrometer made of magnetized iron disks interleaved with plastic scintillators and tracking devices was located downstream of the calorimeter. A momentum resolution of 19% was achieved by magnetic deflection for muons with momenta greater than 7 GeV. At lower momenta, the measurement of the range yielded a 6% resolution.

CHORUS took advantage of the excellent spatial resolution (below 1 μm) of nuclear emulsions. Indeed, at the average energy of the WANF neutrino beam the τ lepton produced in a ν_τ CC interaction travels about 1 mm before its decay. Both the parent track (τ lepton) and the decay product(s) can be seen in the nuclear emulsion and the peculiar decay topology fully reconstructed as shown in Fig. 3. The main advantage with respect to NOMAD is the capability of identifying tau candidates on an event-by-event basis, minimally relying on the kinematic analysis.

As discussed in detail in Ref. [28], the main source of background in the CHORUS experiment originated from the poor efficiency in measuring the momentum and the charge of the decay products. This was mainly due [18] to the limited geometric efficiency of the spectrometer (85%) and to the actual performance of the trackers, which provided a charge discrimination beyond 3σ only for momenta lower than 5 GeV. Indeed, the excellent sensitivity of the nuclear emulsions in detecting also nuclear recoils (which is extremely important in rejecting hadron reinteractions mimicking a decay topology) was partially compromised by the low efficiency in performing the kinematical analysis of the events. The background level achieved (normalized to charged-current interactions) was $\approx 10^{-3}$.

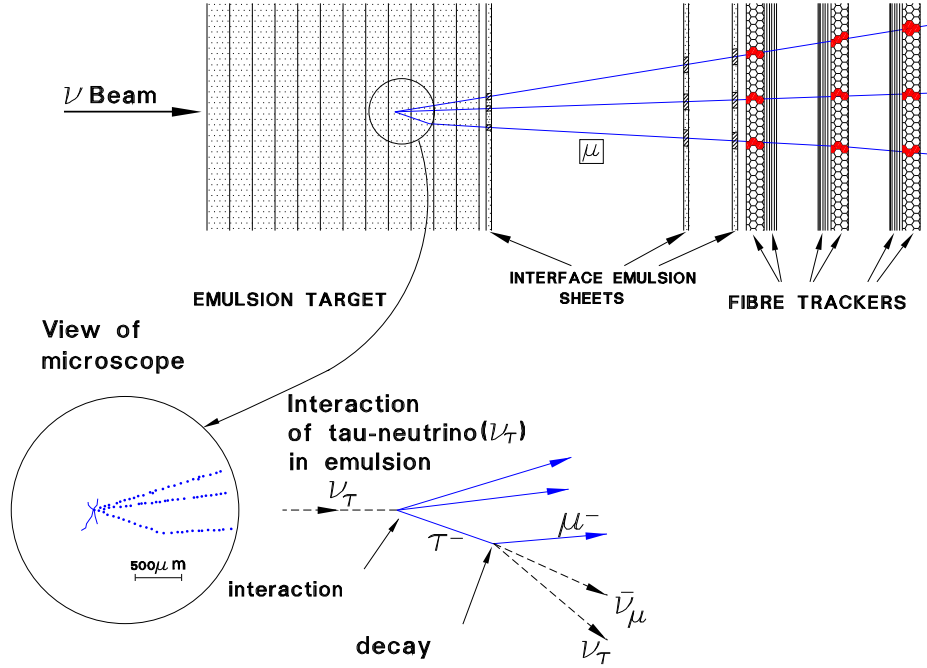


Figure 3. ν_τ detection principle exploited by the CHORUS experiment. A τ lepton produced in a ν_τ CC interaction produces a track of few hundred μm before its decay. The short τ track and the decay product(s) are clearly visible thanks to the excellent spatial resolution of nuclear emulsions.

2.3. CHORUS and NOMAD results

Eventually, both CHORUS [28] and NOMAD [29] had no evidence for $\nu_\mu \rightarrow \nu_\tau$ and $\nu_e \rightarrow \nu_\tau$ oscillations. The 90% C.L. upper limit on the appearance probability was

$$P(\nu_\mu \rightarrow \nu_\tau) < 1.6 \times 10^{-4}.$$

The corresponding limit on the mixing angle is quite stringent; it is $\sin^2 2\theta_{\mu\tau} < 4 \times 10^{-4}$ for large Δm^2 , while the lower Δm^2 value excluded by the two experiments is $\simeq 0.5 \text{ eV}^2$ for maximal mixing (see Fig. 4). It is worth noting that at small mixing angles NOMAD has a better sensitivity, while CHORUS is more sensitive at low Δm^2 . This difference is due to the different experimental techniques employed by the two experiments. NOMAD has been able to collect and analyze a much larger neutrino interaction sample, while CHORUS has higher efficiencies at low neutrino energies.

The study of $\nu_e \rightarrow \nu_\tau$ oscillations was possible thanks to the 0.9% ν_e contamination of the SPS neutrino beam. Assuming that all observable ν_τ would originate from this contamination, the above result translates into a limit on the $\nu_e \rightarrow \nu_\tau$ appearance probability. The difference in energy between the ν_μ ($\langle E_{\nu_\mu} \rangle \sim 26 \text{ GeV}$) and ν_e ($\langle E_{\nu_e} \rangle \sim 42 \text{ GeV}$) components leads to a different shape of the exclusion plot in the oscillation parameter plane. The corresponding 90% C.L. upper limit on the appearance probability is

$$P(\nu_e \rightarrow \nu_\tau) < 1 \times 10^{-2}.$$

The main reason of the large difference in the sensitivity between CHORUS and NOMAD (see Fig. 4) is due to the harder ν_e spectrum with respect to the ν_μ one and to the lower efficiency of CHORUS at high energies.

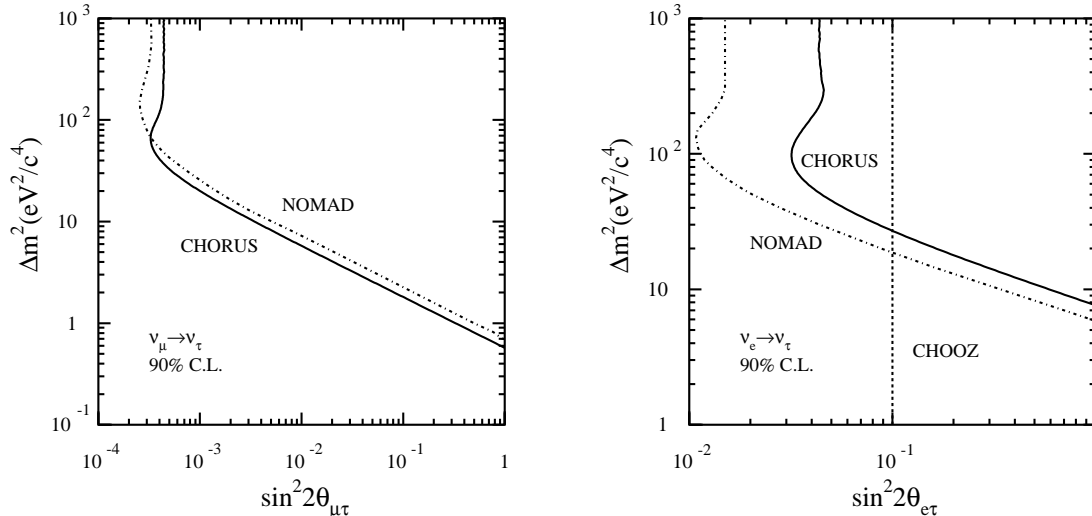


Figure 4. CHORUS (solid lines) and NOMAD (dashed lines) upper limits on $\nu_\mu \rightarrow \nu_\tau$ (left) and $\nu_e \rightarrow \nu_\tau$ (right) oscillation represented in an exclusion plot in the oscillation parameter plane. The latter result is also compared with CHOOZ [9].

3. Evidence from inclusive measurements

Atmospheric neutrinos provided the first convincing evidence for flavor transitions in 1998 [30, 31]. In fact, ν_μ and ν_e produced by the interaction of primary cosmic rays with the nuclei in the earth atmosphere are a powerful discovery tool: their energy spans several order of magnitudes, the flux dropping as $E^{-2.7}$, and oscillations can be probed from medium baselines - $\mathcal{O}(10)$ km for neutrinos produced just above the detector - up to a length comparable with the earth diameter for neutrinos produced on the other side of the earth. The characteristic oscillation frequency due to the squared mass difference of the second and third mass eigenstates (Δm_{32}^2) lies within the atmospheric energy-baseline range and it is prominent in the multi-GeV region. It manifests as a deficit of ν_μ for zenith angles larger than $\pi/2$ (up-going events). This depletion is absent in atmospheric ν_e and, when combined with reactor data, excludes the occurrence of a large $\nu_\mu \rightarrow \nu_e$ conversion, which in turn demonstrates that $\theta_{13} \ll \theta_{23}$. In 2003 this result has been confirmed with artificial sources by the K2K experiment [7] and, more recently, by MINOS [8]. The measurement of MINOS, in particular, provides the most precise measurement to date of Δm_{32}^2 ($\Delta m_{32}^2 = 2.32_{-0.08}^{+0.12} \times 10^{-3} \text{ eV}^2$ [5]). Similarly, atmospheric and accelerator data [32] exclude sizable oscillation probabilities into new types of neutrinos that are singlet under the electroweak gauge group (“sterile

Decay Channel	Branching ratio (%)
$\mu^- \bar{\nu}_\mu \nu_\tau$	17.36 ± 0.05
$e^- \bar{\nu}_e \nu_\tau$	17.85 ± 0.05
$\pi^- \nu_\tau$	10.91 ± 0.07
$h^- \pi^0 \nu_\tau$	25.94 ± 0.09
$h^- \geq 2\pi^0 \nu_\tau$	10.85 ± 0.12
$h^- h^+ h^- \geq 0$ neutrals ν_τ	14.56 ± 0.08

Table 1. Main decay channels for the tau lepton observed in direct appearance searches [12]. h^\pm stands for π^\pm or K^\pm .

neutrinos”) and point toward a disappearance pattern that follows the sinusoidal law characteristic of oscillations [33]. We therefore expect the large disappearance of ν_μ in the multi-GeV range to be due to a large $\nu_\mu \rightarrow \nu_\tau$ transition rate. Such conversion could be revealed in a direct manner by the observation of atmospheric-induced tau leptons from ν_τ CC events occurring in the detector.

Initial state atmospheric neutrinos are almost devoid of ν_τ . Tau neutrinos can be produced by the leptonic decay of D_s in $p+N$ interactions and the level of contamination does not exceed 10^{-6} [34]. In addition, the rate of ν_τ CC interaction is heavily suppressed by the large kinematic threshold and the $E^{-2.7}$ damping factor in the ν_μ spectrum. Assuming the current best fit value of Δm_{32}^2 and maximal atmospheric mixing ($\theta_{23} = \pi/4$ and $\theta_{13} = 0$), about 1 ν_τ CC event/year is expected in a detector with a 1 kton mass [35]. On top of this, the identification of the tau lepton on an event-by-event basis is impossible with coarse-grained detectors as the ones employed for the study of atmospheric neutrinos. The tau lepton decays promptly (lifetime: 291 ± 1 fs) in a variety of final states that are briefly summarized in Table 3. As a consequence, unlike in ν_e and ν_μ CC interactions, the final state lepton in ν_τ CC (the tau) is unobservable in the detector and can only be identified by the topology or kinematics of its decay products. Still, the vast majority of the decays are characterized by a one-prong topology, i.e. one long-living charged particle (e, μ or π^-) accompanied by the large missing energy that is carried by final state neutrinos. This feature is exploited both by inclusive and exclusive measurements (see Sec. 4). Unfortunately, a one-prong + missing energy topology can be easily mimicked by neutral-current (NC) interactions, which represent the dominant background of any inclusive analysis, while the signal-to-noise ratio is ultimately limited by the granularity of the detector.

At the atmospheric scale, evidence for tau appearance has been gained by the SuperKamiokande experiment using water Cerenkov techniques. The huge fiducial mass of the detector (22.5 kton) combined with a decade long exposure compensate the poor signal-to-noise ratio. Larger purities could be obtained by fine-grained detector similar to NOMAD (see Sec. 2) or by homogeneous liquid-Argon TPC’s [36]. Still, the size of these detectors cannot compete with SuperKamiokande: the weight of the largest liquid-Ar detector presently under operation is just 600 tons [37]. Multi-kton liquid-Ar

detectors are, however, considered a viable option to overcome the limitations of water Cherenkov detectors in future atmospheric and long-baseline accelerator experiments. In particular, the opportunities offered by this technology at the 10 kton scale for the inclusive measurement of tau appearance with atmospheric neutrinos has been recently discussed in [38].

The SuperKamiokande Collaboration has published its first analysis on tau appearance in 2006 [35] after an exposure of 1489.2 days (“Super-K I data taking”). The detector consists of two concentric, optically separated regions filled with radiopure water and read-out by large photomultipliers (PMT): the inner region is employed for vertex location and it is equipped with about 11000 20-inch PMT’s (“inner detector”); the outer - readout by sparser 8-inch PMT’s - is used to veto cosmic-ray background, shield neutrons and γ ’s from the surrounding rock (“outer detector”) and identify partially contained events. The overall detector mass is 50 kton but the fiducial volume includes only reconstructed vertices with minimum distance from the walls of the inner detector of 2 m. It corresponds to an effective mass of 22.5 kton. SuperKamiokande identifies charged particles by the corresponding Cherenkov rings in water. In particular, the ν_τ analysis aims at selecting an enriched sample of hadronically decayed tau leptons. Semileptonic tau decays as $\tau \rightarrow \mu\nu_\mu\nu_\tau$ or $\tau \rightarrow e\nu_e\nu_\tau$ are not employed due to the overwhelming background of ν_μ and ν_e CC interactions. Minimum ionizing particles (mainly muons and charged pions) produce sharp ring edges with variable openings, while (ultrarelativistic) electrons and converted photons generate diffused ring patterns with a fixed opening angle of 42° . ν_τ CC interactions occur at $E > 3.5$ GeV and, therefore, are mostly dominated by deep-inelastic scattering. Except for the $\tau \rightarrow \mu\nu_\mu\nu_\tau$ decay channel, most ν_τ events show a multi-ring topology without a leading μ -like (sharp) ring (“e-like sample”). SuperKamiokande has, thus, performed its inclusive analysis in a subsample of events having the vertex located inside the fiducial volume, a visible energy greater than 1.33 GeV and the most energetic ring clearly identified as e-like. This subsample has a signal (ν_τ CC events) to noise ratio of 3% for maximal mixing and $\Delta m_{32}^2 = 2.4 \times 10^{-3}$ eV². Further enrichment can be obtained considering kinematic variables that enhance the difference between tau-like decay topologies and NC or ν_e CC events. In particular, five variables have been considered in [35]: the visible energy, the maximum distance between the primary interaction and electron vertices from pion and then muon decay, the number of rings, the sphericity in the laboratory frame and the clustered sphericity in the center-of-mass frame. Shape information from these variables are combined in a likelihood or, equivalently, in a neural-network output and “tau-like” events are defined as candidates with a likelihood (NN output) greater than 0 (0.5). The tau-like final subsample has a signal-to-noise ratio of about 5%. Although this analysis is in principle strongly dependent on detector simulation, the sample of down-going events provides a unique tool for MC validation. Down-going events are generated by neutrinos that were produced just above the detector, at an average height of 15 km from sea-level if they originate from the decay in flight of π , 13 km if they arise from muon decays. At these baselines the $\nu_\mu \rightarrow \nu_\tau$ probability is negligibly small and, therefore,

they represent a pure sample of unoscillated neutrinos. Evidence of tau appearance can be drawn by the binned fit of the zenith angle (θ) distribution of tau-like events. The fit is done assuming an arbitrary overall normalization (α, β) both for signal (N_i^{τ}) and background (N_i^{bkg}), i.e. minimizing

$$\chi^2 = \sum_{i=1}^n \frac{(N_i^{obs} - \alpha N_i^{\tau} - \beta N_i^{bkg})^2}{\sigma_i^2} \quad (2)$$

σ_i being the statistical error for the i -th bin. A large $\text{Min}(\chi^2)$ for the null hypothesis ($N_i^{\tau} = 0$ for any i) is an indication of regions rich of oscillated ν_{τ} . In fact (see Fig. 3 of Ref. [35]), the zenith distribution shows a rather clear excess of tau-like events in the up-going region, i.e. in the region where oscillations are expected to be large. Thanks to the good knowledge of the leading oscillation parameters Δm_{32}^2 and θ_{23} and to the up/down comparison of the rates, the contributions to the systematic error that in principle should dominate the measurement (the $\sin^2 2\theta_{23}$ factor and the flux overall normalization) mostly cancel out. In fact, systematics are dominated by unknown size of the θ_{13} angle and by the uncertainties on the ν_{τ} cross-section.

A non-zero value of the θ_{13} mixing angle between the first and third family causes a $\nu_{\mu} \rightarrow \nu_e$ conversion that enriches the e-like sample. The enhancement cannot be corrected by the up/down comparison because it is driven by the same phase Δ_{23} as for the leading $\nu_{\mu} \rightarrow \nu_{\tau}$ oscillations and, therefore, builds up only for large baselines (up-going). Note also that the systematic shift due to θ_{13} is asymmetric since, for any value of the angle, it always causes an apparent increase of the statistics of up-going events. SuperKamiokande estimated this effect to be smaller than 21%. The estimate relies on the present best limit on θ_{13} from the CHOOZ experiment ($\sin^2 \theta_{13} < 0.027$ at 90% CL [9, 39]). Since the measurements of θ_{13} by reactor or long-baseline experiments are uncorrelated with the atmospheric measurement, a significant improvement of this systematics is expected in the next few years, taking advantage of the results from Double-CHOOZ [40], RENO [41], T2K [42], Daya Bay [43] and NO ν A [44]. The effect being proportional to $\sin^2 2\theta_{13}$, we expect such systematics to drop at the level of a few percent in less than 5 years. On the contrary, no major improvements can be anticipated from the other dominant contribution, i.e. the knowledge of the ν_{τ} cross-section. Although this number is immaterial when testing against the no-appearance (null) hypothesis (i.e. the hypothesis corresponding to no evidence for taus in the enriched sample), it is of relevance in order to compare the data to the expected rate within the standard three-family oscillation framework. SuperKamiokande is particularly sensitive to the uncertainty in the cross-section because the oscillated tau-events are mostly at low energy, i.e. in the proximity of the sharp rise of the cross-section just beyond the kinematic threshold. This effect is due to the $E^{-2.7}$ cutoff of the unoscillated ν_{μ} spectrum. SuperKamiokande estimated this contribution to be smaller than 25% by comparison among different theoretical models [45].

The 2006 (SuperK-I) analysis provided evidence for tau appearance at the 2.4 sigma level, the best fit of the signal in the tau-like sample being $138 \pm 48(\text{stat})_{-32}^{+15}(\text{sys})$. A

priori, the expected sensitivity was about 2 sigma and a larger rejection power against the null hypothesis has been reached thanks to the larger number of observed events.

In 2001, during the refill after a shutdown aimed at replacing dead photomultipliers (PMT), an accident occurred in the SuperKamiokande detector, which caused the loss of about 60% of the photodetectors. The remaining 20-inch PMT were redeployed in the inner detector (ID) while the PMT of the outer veto were fully rebuilt. In this configuration, which is clearly not optimal for inclusive tau search due to the reduced ID coverage (47% of the original one) SuperKamiokande took data until 2005 (“SuperK-II”). Still, the atmospheric results obtained during SuperK-II are in good agreement with previous results both in the disappearance [46] and in the appearance [47] analyses. The repair of SuperKamiokande was completed in July 2006 and, since then, full coverage at the inner detector has been restored (“SuperK-III data taking”). The data taking of this third phase was completed in 2008 and the preliminary SuperK-I,II,III combined data have been presented in December 2010 [48]. SuperK-III adds 518 days of statistics at nominal coverage; moreover, the inclusive tau appearance analysis has been improved. It now employs a 2-D unbinned likelihood fit that uses the complete distribution of the neural-network output instead of a sharp cut (> 0.5) to distinguish between background-like and tau-like topologies. It also makes use of a modified set of inclusive variables with higher sensitivity. The overall expected sensitivity of the new analysis computed from simulation and assuming nominal cross-sections is significantly better than the one of 2006 (2.6σ versus 2σ). On top of this, a larger enhancement has been observed in the up-going sample with respect to the down-going reference data. Such enhancement excludes the null hypothesis (no tau oscillation) at the 3.8σ level. If these preliminary results are confirmed, we can safely expect that inclusive measurements will dominate the experimental evidence for $\nu_\mu \rightarrow \nu_\tau$ transitions in the next few years, before the final results from CNGS.

4. Evidence from exclusive measurements

Inclusive analyses try to distill a tau-enriched sample in the bulk of ν_μ and ν_e interactions and take advantage of the large statistics and of the peculiar kinematics of tau decays. Exclusive measurements are even more ambitious since they aim at observing the appearance of tau leptons on an event-by-event basis. It necessarily requires a detector with very high spatial resolution, such as to observe the decay in flight of the tau and, at the same time, a high intensity source with an energy well exceeding the kinematic threshold for tau production. The only facility that is able to fulfill simultaneously these requirements is the CNGS facility in Europe. The CNGS beam [49] is a pure ν_μ beam with a mean energy of 17 GeV produced at CERN and pointing to the Gran Sasso Laboratories of INFN in Italy (LNGS), 730 km away from the source. The intrinsic ν_τ contamination, mainly originating from the decay of D_s , is negligible ($< 10^{-6}$). The beam is also contaminated at the 0.8% by ν_e , resulting from the decay in flight of muons along the decay tunnel and from K_{e3} decays. Since the tau lepton is identified from its

decay topology, background from prompt ν_e is irrelevant.

The observation of tau leptons at the far detector will thus prove unambiguously that the $\nu_\mu \rightarrow \nu_\tau$ oscillation is the dominant transition channel at the atmospheric scale. This is the main goal of the OPERA experiment [50, 51, 52], which has been built from 2004 to 2008 [53] in the Hall C of LNGS as a far detector for CNGS.

In OPERA, the ν_τ appearance signal is detected through the measurement of the decay daughter particles of the τ lepton produced in CC ν_τ interactions. Since the short-lived τ particle has an average decay length of about 1 mm at the CNGS beam energy, a micrometric detection resolution is needed. In OPERA, neutrinos interact in a large mass target made of lead plates interspaced with nuclear emulsion films acting as high-accuracy tracking devices. This kind of detector is historically called an Emulsion Cloud Chamber (ECC) and it has been successfully applied by the DONUT experiment to perform the first direct observation of ν_τ charged-current interactions in a ν_τ enriched beam at Fermilab [54].

OPERA is a hybrid detector [55] (see Fig. 5) made of a veto plane followed by two identical Super Modules (SM). Each SM consists of a target section of about 625 tons made of 75000 emulsion/lead ECC modules, or "bricks", of a scintillator Target Tracker detector (TT) to trigger and localize neutrino interactions within the target, and of a muon spectrometer. A target brick consists of 56 lead plates of 1 mm thickness interleaved with 57 emulsion films and with a mass of 8.3 kg. Their thickness along the beam direction corresponds to about 10 radiation lengths. In order to reduce the emulsion scanning load, Changeable Sheet (CS) films have been used. They consist of tightly packed doublets of emulsion films glued to the downstream face of each brick.

Charged particles from a neutrino interaction in a brick cross the CS and produce signals in the TT that allow the corresponding brick to be identified and extracted by an automated system. The hit patten in the TT provides information on the bricks where the neutrino interaction has occurred. The brick with the largest probability to contain the vertex is, hence, extracted and its CS is detached, developed and scanned. If tracks are found in the CS matching the expectation from TT, the brick is developed and the tracks are traced back up to the interaction vertex. Otherwise the procedure is repeated for the second most probable brick.

Large ancillary facilities are used to bring bricks from the target up to the automatic scanning microscopes at LNGS and various laboratories in Europe and Japan [56, 57]. Extensive information on the OPERA detector and its support facilities are given in [55, 58].

A reconstructed CC event is shown in the bottom panels of Fig. 6. In this case the dimensions of the event views are of the order of a few millimeters, to be compared with the ~ 10 m scale of the whole event reconstructed with the electronic detectors (top panels of Fig. 6).

As mentioned before, the CNGS beam is optimized for the observation of ν_τ CC interactions. The average neutrino energy is ~ 17 GeV. The $\bar{\nu}_\mu$ CC contamination is 2.1%; the ν_e and $\bar{\nu}_e$ contaminations are less than 1% and, as noted above, the number

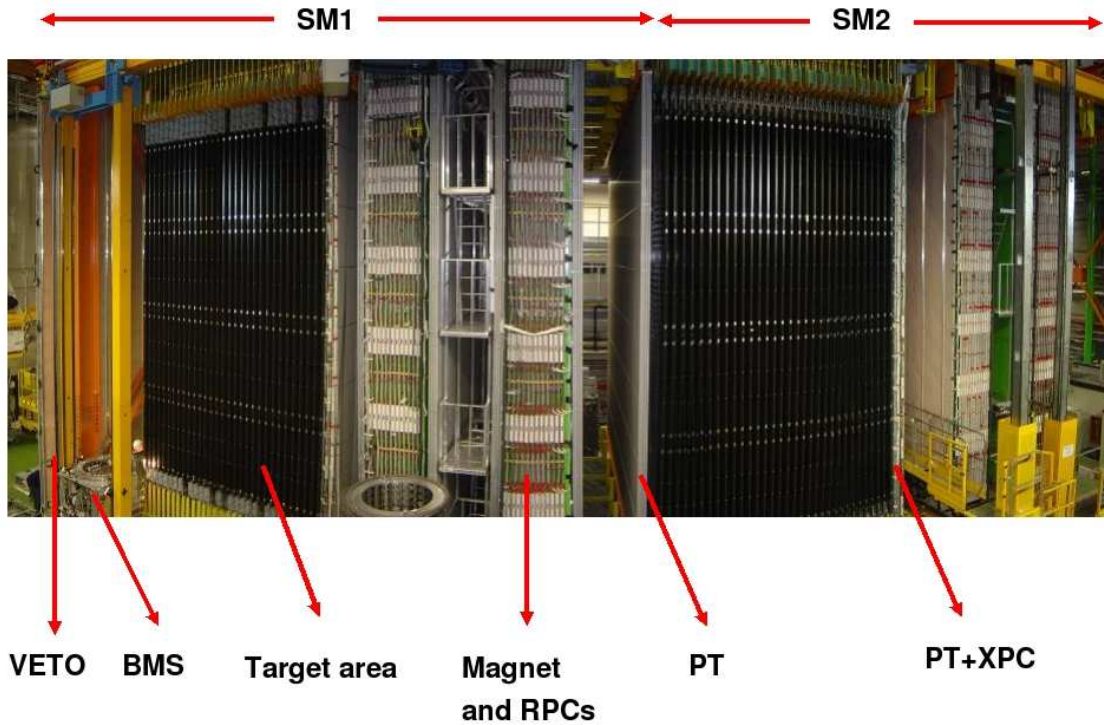


Figure 5. View of the OPERA detector. The upper horizontal lines indicate the position of the two identical supermodules (SM1 and SM2). The “target area” is made of walls filled with ECC bricks interleaved with planes of plastic scintillators. Arrows show the position of the VETO planes, the drift tubes (PT) pulled alongside the XPC, the magnets and the Resistive Plate Chambers (RPC) installed between the magnet iron slabs. The XPC are RPC planes with redout strips inclined by 45° with respect to the horizontal. The Brick Manipulator System (BMS) is also visible.

of prompt ν_τ is negligible. With a total CNGS beam intensity of 22.5×10^{19} protons on target (p.o.t.), about 24300 neutrino events would be collected.

The τ decay channels investigated by OPERA cover all the decay modes. Indeed, the e , μ , single-prong (lines 3-5 of Table 3) and multi-prong (line 6 of Table 3) decays are measured. They are classified in 2 categories: “long” and “short” decays. Short decays correspond to the cases when the τ decays in the same lead plate in which the neutrino interaction occurred. The τ candidates are selected on the basis of the impact parameter of the τ daughter track with respect to the interaction vertex ($IP > 5\text{-}20 \mu\text{m}$). In the long decay category the τ does not decay in the same lead plate and its track can be reconstructed in one film. The τ candidate events are selected either on the basis of the existence of a kink angle between the τ and the daughter tracks ($\theta_{kink} > 20 \text{ mrad}$) or on the presence of a secondary multi-prong vertex along the τ track.

In order to improve the signal to background ratio, a kinematical analysis is applied

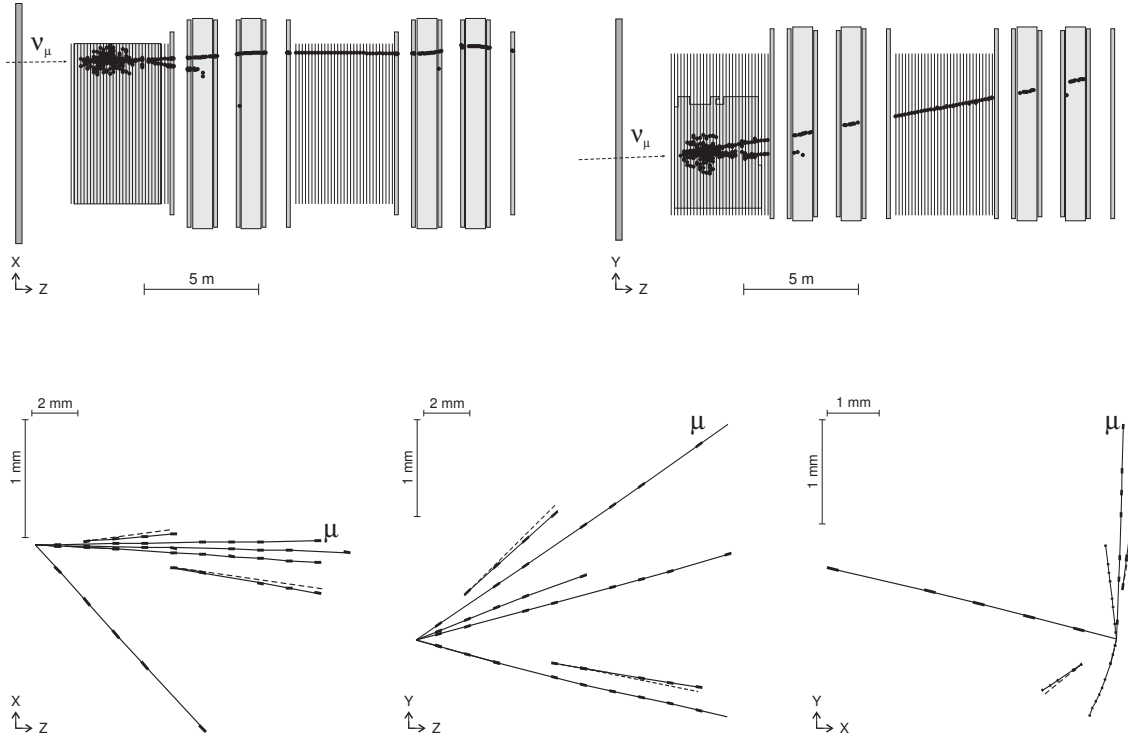


Figure 6. Top panels: on line display of an event seen by the OPERA electronic detectors (side and top views): a ν_μ interacts in one of the first bricks of the first supermodule (SM) yielding hadrons and a muon which is detected in both SMs and whose momentum is measured by the magnets of the two SMs. Bottom panels: the vertex of the same event observed in the emulsion films (side, top and front views). Note the two $\gamma \rightarrow e^+e^-$ vertices: the opening angle between them is about 300 mrad. By measuring the energy of the γ 's one obtains a reconstructed invariant mass of 110 ± 30 MeV, consistent with the π^0 mass.

to τ candidates selected on the basis of the topological criteria discussed above. Since for short decay candidates the main background comes from charm production, a lower cut at 2 GeV on the invariant mass of the hadronic system is imposed. This cut reduces the background by more than a factor 1000, while retaining about 15% of the signal. For long decay candidates it is worthwhile to consider leptonic, single-prong and multi-prong decays separately. For leptonic decays soft cuts on the daughter momentum, a lower one to minimize the effect of the particle misidentification ($p > 1$ GeV) and an upper one ($p < 15$ GeV) to suppress the beam related background (ν_e from the beam and the high energy ν_μ tail of CNGS), and a soft cut on the measured transverse momentum (p_T) at the decay vertex are enough to reduced a background at a reasonable level. The applied cut at the decay vertex is $p_T > 100$ MeV and $p_T > 250$ MeV for the electronic and muonic decay channel, respectively.

For the single-prong decay the kinematical analysis is slightly more complicated. The main background for this channel originates from the reinteraction of primary hadrons without any visible recoil at the reinteraction vertex. In order to keep the

background for this channel as low as possible kinematical cuts are applied both at the decay and at the primary vertex. The kinematical analysis is qualitatively similar to that of the electronic and muonic channels. However, the cut applied on the p_T is harder ($p_T > 300$ MeV if a γ is attached to the decay vertex, $p_T > 600$ MeV if not) and the daughter particle is required to have a momentum larger than 2 GeV. The kinematical analysis at the primary vertex uses the variables p_T^{miss} , defined as the missing transverse momentum at the primary vertex, and ϕ , which is the angle in the transverse plane between the parent track and the shower direction. Due to the unobserved outgoing neutrino, p_T^{miss} is expected to be large in NC interactions. Conversely, it is expected to be small in CC interactions. For τ candidates the measured p_T^{miss} is required to be lower than 1 GeV. The ϕ angle is expected to peak at π , because the τ and the hadronic shower are back-to-back in the transverse plane. On the contrary, the hadron mimicking a $\tau \rightarrow h$ decay is produced inside the hadronic shower in NC interactions. Therefore, ϕ peaks near 0 and for τ candidates the ϕ angle is required to be larger than $\pi/2$.

For the multi-prong decay channel the main background is given by multi-prong decay of charmed particles. The hadronic reinteraction background is not a major issue. Indeed, the probability for a hadron to undergo an interaction with multi-prong is much smaller (1-2 order of magnitudes) than for single-prong interactions. The signal to background ratio is enhanced by performing a kinematical analysis mainly based on the following variables: p_T^{miss} , defined as the missing transverse momentum at the primary vertex, the invariant mass of the hadronic system, the total energy of the event.

In Ref [59] the OPERA Collaboration reported the observation of a first candidate ν_τ CC interaction in the detector. The primary neutrino interaction consists of 7 tracks of which one exhibits a visible kink. Two electromagnetic showers due to γ -rays have been located; they are clearly associated with the event and were produced at the decay vertex. Fig. 7 shows a display of the event, which was identified in a sample corresponding to 1.89×10^{19} p.o.t. in the CNGS ν_μ beam. The total transverse momentum P_T of the daughter particles with respect to the parent track is $(0.47^{+0.24}_{-0.12})$ GeV, above the lower selection cut-off at 0.3 GeV. The missing transverse momentum P_T^{miss} at the primary vertex is $(0.57^{+0.32}_{-0.17})$ GeV. This is lower than the upper selection cut-off at 1 GeV. The angle Φ between the parent track and the rest of the hadronic shower in the transverse plane is equal to (3.01 ± 0.03) rad, largely above the lower selection cut-off fixed at $\pi/2$. The invariant mass of γ -rays is $(120 \pm 20(stat.) \pm 35(syst.))$ MeV², supporting the hypothesis that they originate from a π^0 decay. Similarly the invariant mass of the charged decay product assumed to be a π^- and of the two γ -rays is $(640^{+125}_{-80}(stat.)^{+100}_{-90}(syst.))$ MeV, which is compatible with the $\rho(770)$ mass. The branching ratio of the decay mode $\tau \rightarrow \rho^- \nu_\tau$ is about 25%. The observation of one possible tau candidate in the decay channel $h^-(\pi^0)\nu_\tau$ has a significance of 2.36σ of not being a background fluctuation from a background of 0.018 ± 0.007 . If one considers all decay modes included in the search, corresponding to 0.54 ± 0.13 expected taus, the significance of the observation becomes 2.01σ from the total predicted background of 0.045 ± 0.023 .

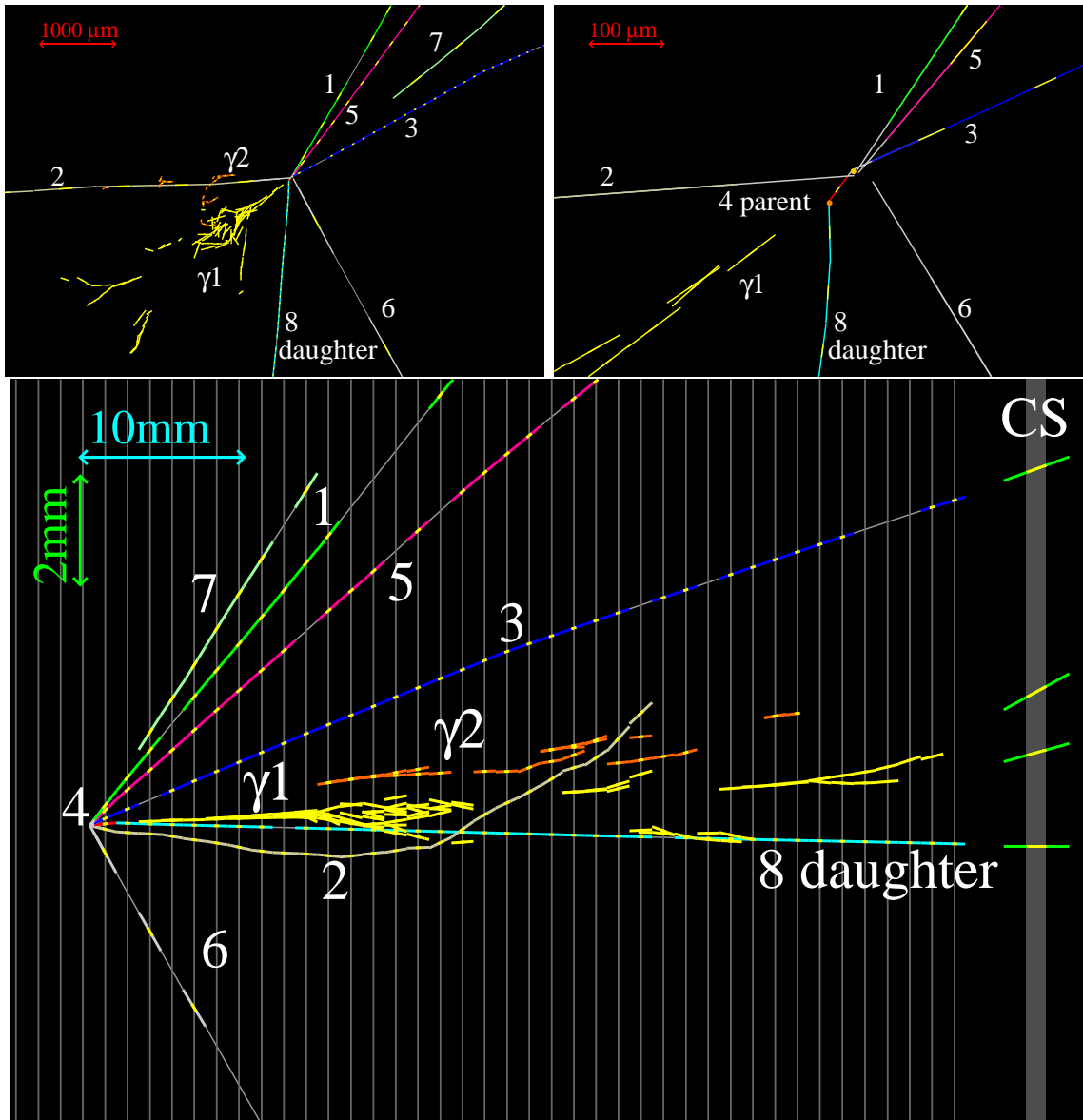


Figure 7. Display of the τ^- candidate event. Top left: view transverse to the neutrino direction. Top right: same view zoomed on the vertices. Bottom: longitudinal view.

5. Future experiments

5.1. Tau appearance in the standard oscillation scenario

The role of tau appearance for a direct proof of oscillation is unique. In the standard three-family framework, precision measurements of the leading oscillation parameters θ_{12} , θ_{23} , Δm_{21}^2 and Δm_{32}^2 , can be done more easily studying the disappearance of solar+reactor ν_e and atmospheric+accelerator ν_μ . Similarly, the unknown angle θ_{13} and the CP violating phase δ will likely be addressed studying subdominant $\nu_\mu \rightarrow \nu_e$ (or $\nu_e \rightarrow \nu_\mu$) oscillations at the atmospheric scale. This is the reason why there are no

facilities that have been pursued since 1998 and that are specifically tuned for precision measurements of $\nu_\mu \rightarrow \nu_\tau$ transitions. In fact, among the many setups proposed to study CP violation in the leptonic sector, just a few [60, 61] work beyond the kinematic threshold for tau production. The most prominent are the Neutrino Factories [60], where neutrinos are produced by the decay-in-flight of muons or antimuons. (Anti)muons produce final-state neutrinos from the decay $\mu^+ \rightarrow e^+ \bar{\nu}_\mu \nu_e$. The neutrino factories allow for the study of the transition $\nu_e \rightarrow \nu_\mu$ if one identifies the signal of “wrong-sign” muons coming from ν_μ CC events in the bulk of “right-sign” muons originating from $\bar{\nu}_\mu$ CC interactions. As a consequence, the most natural far detector for the neutrino factory is a high-density magnetized calorimeter [62] with outstanding charge reconstruction capabilities. The need of charge identification efficiencies well above 99.9% requires a strong muon energy cut to filter punch-through pions or pions that have decayed in flight. In the classic high energy Neutrino Factory configuration [63, 64], 50 GeV muons are accelerated and stacked in a decay ring, producing ν_e of ~ 30 GeV energy. In order to achieve charge misidentification of $\mathcal{O}(10^{-4})$, a tight muon energy cut is applied so that the detector efficiency drops to zero at energies below 10 GeV. For typical baselines of 2000 km, it means that the peak of the oscillation (neutrinos where $\Delta m_{32}^2 L/4E \simeq \pi/2$) remains completely unobserved in the Neutrino Factories, as well as in CNGS. Such tight cut is the origin of one of the main drawback of the Neutrino Factories: unlike more traditional setups that study $\nu_\mu \rightarrow \nu_e$ transitions at the oscillation peak (“Superbeams”), a strong parameter degeneracy appears once we go from the measurement of the $\nu_\mu \rightarrow \nu_e$ and $\bar{\nu}_e \rightarrow \bar{\nu}_\mu$ probabilities to the determination of the δ and θ_{13} angles (“intrinsic degeneracy” [65]). The degeneracy is particularly severe for $\sin^2 2\theta_{13} \simeq 10^{-3}$, i.e. in a region where the performance of the Neutrino Factory should be unbeatable with respect to Superbeams [63] or Betabeams [66]. Tau appearance can help to overcome this drawback, at the price of a dedicated detector located at a shorter baseline and specifically aimed at observing $\nu_e \rightarrow \nu_\tau$ transitions.

In fact, an emulsion based detector similar to OPERA can perform this measurement identifying “wrong-sign” muons in the magnetic spectrometer and tracing back the particle up to lead-emulsion or iron-emulsion bricks to observe the appearance of a decay kink [67]. The pattern of $\nu_e \rightarrow \nu_\tau$ ($P_{e\tau}$) closely resembles the one of $\nu_e \rightarrow \nu_\mu$ ($P_{e\mu}$). If we expand the ν_μ appearance probability to second order in $\sin 2\theta_{13}$ and the hierarchy parameter $\alpha \equiv \Delta m_{21}^2/\Delta m_{31}^2 \simeq 0.03$ [68], we get

$$\begin{aligned}
P_{e\mu} &\simeq \sin^2 2\theta_{13} \sin^2 \theta_{23} \frac{\sin^2[(1 - \hat{A})\Delta_{31}]}{(1 - \hat{A})^2} \\
&\pm \alpha \sin 2\theta_{13} \sin \delta \sin 2\theta_{12} \sin 2\theta_{23} \sin(\Delta_{31}) \frac{\sin(\hat{A}\Delta_{31}) \sin[(1 - \hat{A})\Delta_{31}]}{\hat{A} (1 - \hat{A})} \\
&+ \alpha \sin 2\theta_{13} \cos \delta \sin 2\theta_{12} \sin 2\theta_{23} \cos(\Delta_{31}) \frac{\sin(\hat{A}\Delta_{31}) \sin[(1 - \hat{A})\Delta_{31}]}{\hat{A} (1 - \hat{A})} \\
&+ \alpha^2 \cos^2 \theta_{23} \sin^2 2\theta_{12} \frac{\sin^2(\hat{A}\Delta_{31})}{\hat{A}^2}; \tag{3}
\end{aligned}$$

here, $\Delta_{31} \equiv \Delta m_{31}^2 L / (4E)$ and $\hat{A} = \pm 2\sqrt{2} E G_F n_e / \Delta m_{31}^2$, G_F and n_e being the Fermi constant and the electron density in the earth crust, respectively. The signs in the second term and \hat{A} are positive for neutrinos and negative for anti-neutrinos. On the other hand, in $P_{e\tau}$ the sign of the second and third terms are flipped and the replacement $\sin^2 \theta_{23} \leftrightarrow \cos^2 \theta_{23}$ takes place in the first and fourth terms. In particular, for maximal atmospheric mixing only the signs of the second and third terms change. As a consequence, the measurement of the “golden channel” $\nu_e \rightarrow \nu_\mu$, of its CP conjugate $\bar{\nu}_e \rightarrow \bar{\nu}_\mu$ and of the additional transition $\nu_e \rightarrow \nu_\tau$ (“silver channel”) can solve the intrinsic degeneracy for values of θ_{13} larger than 1° and $\simeq 5$ kton of detector mass [69].

More recently, it has been pointed out that a significant improvement of the Neutrino Factory performance could be achieved relaxing the energy cut to smaller values and putting up with a worse charge identification efficiency below 10 GeV [70, 71]. In this region, however, tau appearance still plays an important role [72]. For coarse-grained detectors such as magnetized iron calorimeters, the golden channel is highly contaminated by unidentified silver channel events [73], i.e. $\nu_e \rightarrow \nu_\tau$ transitions where the tau decays in $\mu\bar{\nu}_\mu\nu_e$. The detector reconstructs the events as standard “wrong sign” muons although the actual neutrino energy shows poor correlation with the measured muon momentum, due to the large missing energy in $\tau \rightarrow \mu\bar{\nu}_\mu\nu_e$. Hence, the silver channel populates the golden signal region as a broad-band background and introduces a large systematic error in the extraction of θ_{13} and the CP violating phase [73]. Still, once the silver channel “background” is accounted for in the fits of the golden event spectra, the correct values of the parameters can be recovered [71] and, in addition, the problem of the degeneracies is further relieved due to the lowering of the muon energy cut. Clearly, consistency among these spectra, which entangles subdominant $\nu_e \rightarrow \nu_\tau$ and $\nu_e \rightarrow \nu_\mu$ oscillations would be an impressive test for the standard three-family interpretation of leptonic mixing, even without an explicit observation of a $\nu_e \rightarrow \nu_\tau$ sample.

5.2. τ appearance and Non Standard Interactions

Mass-generation mechanisms for neutrinos naturally produce perturbations in the Standard Model couplings of these particles, referred to as non-standard interactions (NSI). Broadly speaking, NSI can manifest themselves in two different ways. If they perturb charged-currents they can affect neutrino production and detection, conversely if they modify neutral-currents they affect neutrino propagation.

If we consider NSI in the production and detection mechanisms, then the NSI themselves can be parametrized as a small mixture of the wrong flavor ν_β to a neutrino produced or detected in association with a charged lepton α , i.e.

$$\nu'_\alpha = \nu_\alpha + \sum_{\beta=e,\mu,\tau} \varepsilon_{\alpha\beta} \nu_\beta, \quad (4)$$

where the parameters ε give the strength of the NSI relative to the standard weak interactions. Here, a short distance between the source and the detector is mandatory

in order to minimize the oscillation probability and, therefore, enhance the NSI contribution. On the other hand, long baseline neutrino experiments mainly constrain NSI affecting NC since these NSI perturb neutrino oscillation in matter at macroscopic distances. In this case, NSI appear in the Hamiltonian describing neutrino propagation in matter:

$$\mathcal{H} = \frac{1}{2E} U \begin{pmatrix} 0 & 0 & 0 \\ 0 & \Delta m_{21}^2 & 0 \\ 0 & 0 & \Delta m_{31}^2 \end{pmatrix} U^\dagger + \frac{1}{2E} \begin{pmatrix} V & 0 & 0 \\ 0 & 0 & 0 \\ 0 & 0 & 0 \end{pmatrix} + \mathcal{H}_{NSI}, \quad (5)$$

where U is the leptonic mixing matrix and $V = \sqrt{2}G_F n_e$ is the contribution arising from ordinary matter effects (Mikheyev-Smirnov-Wolfenstein effect [74]), G_F being the Fermi constant and n_e the density of electrons in the medium.

NSI can be simply induced by non-unitarity of the leptonic mixing matrix - e.g., in see-saw models - or caused by one-loop exchange of new particles - e.g., by spinless bosons in supersymmetric models [75]. If the scale of new physics is high, these effects are small but models where NSI are significantly enhanced are possible and have been investigated in the literature. In the 90's the study of these models was boosted by a possible non-oscillation explanation of the solar neutrino puzzle [76]. In recent years, both the hint for a non-zero value of θ_{13} from solar data and the Miniboone anomalies [77, 78] have revived the interest on NSI, which can now act as a subdominant contribution to neutrino oscillations [79, 80, 81]; as a consequence, a precision measurement campaign is considered mandatory. Since precision oscillation physics is a young field of research, limits on NSI affecting the propagation of neutrinos are rather loose. On the other hand, more stringent bounds can be drawn from processes that involve the production and detection of neutrinos in short baseline experiments or radiative contributions to rare decays [82].

Even accounting for short baseline experiments, present model independent bounds on ε are quite loose - $\mathcal{O}(0.1 - 1)$. Here, a new generation of high precision experiments at short baselines would represent the ideal tool to probe much smaller values of ε .

A clear evidence for NSI working at production and detection would be the measurement of a non-unitarity [83] of the leptonic mixing matrix. A possible approach to investigate the non-unitarity is to measure all oscillation probabilities $P(\nu_\mu \rightarrow \nu_\mu)$, $P(\nu_\mu \rightarrow \nu_e)$, $P(\nu_\mu \rightarrow \nu_\tau)$ (or $P(\nu_e \rightarrow \nu_\mu)$, $P(\nu_e \rightarrow \nu_e)$, $P(\nu_e \rightarrow \nu_\tau)$) and check that they sum up to one. In this case the best approach would be to build a dedicated near detector to measure all oscillation channels.

Indeed, neutrino oscillations constitute an irreducible background for such possible rare processes. Nevertheless, the short-baseline choice has the drawback that the NSI signal is given by the product of the production and detection mechanisms. In order to disentangle the two mechanisms it is important to exploit different neutrino sources and as many final states as possible. In this respect, it is useful to exploit high-energy neutrino beams where the τ production yield increases with the neutrino energy and, therefore, final states with τ leptons can be studied. This consideration motivated proposals [84] for a new generation of short-baseline experiments in tau appearance

mode. They are aimed at precisions better than 10^{-6} to investigate theory-driven enhancements of NSI: at these baselines, the dominant contributions come from the production/detection of neutrinos while propagation effects are negligible.

If the propagation mechanism is affected by NSI, then long baseline experiments are necessary. In general, these experiments compete with the information that can be drawn from current atmospheric data [79, 85], but the purity of the source can be fruitfully employed to tighten some bounds. In particular, tau appearance in OPERA can be used to improve our knowledge of $\epsilon_{\mu\tau}$ [86] § while the CNGS statistics is too poor to impact bounds on $\epsilon_{\tau\tau}$ or $\epsilon_{e\tau}$ [87]. Large statistics tau appearance experiments where matter effects are dominant and, therefore, NSI due to propagation are sizable, are possible only in the framework of the Neutrino Factories (see Sec. 5.1). A systematic assessment of performance of these facilities with respect to NSI has been carried out in [88]. Here, the use of the tau appearance channel, the “silver channel” of Sec. 5.1, is relevant only for high energy neutrino factories with muon energies larger than ~ 25 GeV and its sensitivity is mainly limited to $\epsilon_{e\tau}$.

5.3. τ appearance and sterile neutrinos

The possible confirmation of the LSND anomaly [89] by the MiniBoone antineutrino data [78] makes the study of hypothetical neutrinos that are singlet under the electroweak gauge groups, sterile neutrinos, a very lively field of research. It is, therefore, interesting to assess the contribution of the tau appearance channel to the clarification of this issue, at least in the simplest scenarios where just one sterile neutrino is added to the three active families, the 3+1 scheme. Unfortunately, this oversimplified scheme is not able to account for all experimental data and the current global fit is very poor. More sophisticated models (see e.g.,[90]) show better agreement with data but the 3+1 scheme illustrates very well the experimental challenges. Moreover, many of the considerations made in Sec. 5.2 hold for sterile neutrino searches, too. The impact of $\nu_\mu \rightarrow \nu_\tau$ appearance searches in the framework of the 3+1 scheme has been studied for both conventional [91] and Neutrino Factory beams [92, 93]. In the first case, if the OPERA detector is exposed to the nominal CNGS beam intensity, a null result can slightly improve the present bound on θ_{13} || but not those on the active-sterile mixing angles, θ_{14} , θ_{24} and θ_{34} . If the beam intensity is increased by a factor 2 or beyond, not only the sensitivity to θ_{13} increases accordingly, but a significant sensitivity to θ_{24} and θ_{34} can be achieved. The θ_{24} and θ_{34} sensitivities strongly depend on the value of the CP-violating phase δ_3 , highest sensitivities being available for $\delta_3 \simeq \pi/2$. In order to reach significant improvements on θ_{13} , the angle should better be constrained by high-intensity ν_e disappearance experiments. Once more (see Sec. 5.2), OPERA is limited by the small detector mass. It is, however, very interesting to note that the sensitivity

§ For a definition of the ϵ couplings relevant for neutrino propagation, see e.g. [79].

|| This angle is different from the θ_{13} angle defined in Sec.1. It represents the mixing angle between the first and third family in a 3 active + 1 sterile neutrino mixing scheme.

of OPERA to θ_{13} and to the other angles of the 3+1 model mainly comes from the study of $\nu_\mu \rightarrow \nu_\tau$ transitions, while the corresponding sensitivity due to $\nu_\mu \rightarrow \nu_e$, the CP conjugate of the LSND measurement, is marginal. This is due to the rather large baseline compared with LSND/Miniboone and to the additional constraints coming from the SuperKamiokande atmospheric data.

Clearly, the results that can be obtained at a Neutrino Factory are much better than those obtained by exploiting the CNGS beam, even assuming a major upgrade of the facility [91]. As for the case of the silver channel (Sec. 5.1), the setup must be equipped with a massive OPERA-like detector; the ideal baseline is, nevertheless, ~ 3000 km, i.e. the detector can be positioned in the same underground site as for the magnetized calorimeter. In this case, the detector seeks for “right-sign” muons in coincidence with a decay kink, i.e. it measures the leading $\nu_\mu \rightarrow \nu_\tau$ transition, which is sometimes called the “discovery channel”, in contrast with the $\nu_e \rightarrow \nu_\tau$ silver channel of Sec. 5.1. Further improvements can be achieved exploiting Magnetized Emulsion Cloud Chambers [94, 95] made of iron bricks and photographic films. The magnetization of the iron allows for sign measurement of the final state particles even in the occurrence of muon-less tau decays. A viable alternative to the study of tau appearance seems, however, the exploitation of near detectors located close to the muon decay ring [93], especially if $\Delta m_{41} \gg \Delta m_{31}$.

6. Conclusions

The search for an explicit observation of flavor changing neutrino oscillations by identifying a different lepton than the one of the initial flavor has a decades long history. In 1998 it became clear that the bulk of oscillations at the atmospheric scale is likely constituted by $\nu_\mu \rightarrow \nu_\tau$ transitions: this consideration has boosted enormously the search for tau appearance in long-baseline experiments both with natural and artificial sources. Between 2006 and 2010, SuperKamiokande and OPERA have gained evidence of such transition using quite different techniques and significant improvements are expected in the next few years. Although no dedicated facilities for precision measurements of tau appearance have been designed so far, it is clear that the study of $\nu_\mu \rightarrow \nu_\tau$ will play a relevant role in any experiment operating beyond the kinematical threshold for tau production and especially in the far detectors of the Neutrino Factories. Novel short-baseline experiments along the line of CHORUS and NOMAD can be of interest beyond the standard three-family oscillation scenario, mainly for precision searches of non-standard interactions.

Acknowledgments

We wish to express our gratitude to Andrea Donini, Antonio Ereditato and Chris Walter for many useful discussions and careful reading of the manuscript.

References

- [1] C. Giunti, C. W. Kim, “Fundamentals of Neutrino Physics and Astrophysics,” Oxford University Press, Oxford, UK, 2007.
- [2] B. Pontecorvo, Sov. Phys. JETP **6** (1957) 429 [Zh. Eksp. Teor. Fiz. **33** (1957) 549]; B. Pontecorvo, Sov. Phys. JETP **6** (1968) 984 [Zh. Eksp. Teor. Fiz. **53** (1967) 1717].
- [3] Y. Katayama, K. Matunoto, S. Tanaka and E. Yamada, Progr. Theor. Phys. **28** (1962) 675; Z. Maki, M. Nakagawa and S. Sakata, Prog. Theor. Phys. **28** (1962) 870; B. Pontecorvo, Sov. Phys. JETP **26** (1968) 984 [Zh. Eksp. Teor. Fiz. **53** (1967) 1717]; V. N. Gribov and B. Pontecorvo, Phys. Lett. B **28** (1969) 493.
- [4] T. Schwetz, M. A. Tortola and J. W. F. Valle, New J. Phys. **10** (2008) 113011.
- [5] P. Adamson *et al.* [The MINOS Collaboration], “Measurement of the neutrino mass splitting and flavor mixing by MINOS,” arXiv:1103.0340 [hep-ex].
- [6] S. Abe *et al.* [KamLAND Collaboration], Phys. Rev. Lett. **100** (2008) 221803.
- [7] M.H. Ahn *et al.* [K2K Coll.], Phys. Rev. Lett. **90** (2003) 041801; M. H. Ahn *et al.* [K2K Collaboration], Phys. Rev. D **74** (2006) 072003.
- [8] D. G. Michael *et al.* [MINOS Collaboration], Phys. Rev. Lett. **97** (2006) 191801. P. Adamson *et al.* [MINOS Collaboration], Phys. Rev. **D77** (2008) 072002; P. Adamson *et al.* [MINOS Collaboration], Phys. Rev. Lett. **101** (2008) 131802.
- [9] M. Apollonio *et al.* [CHOOZ Collaboration], Eur. Phys. J. C **27** (2003) 331.
- [10] F. Boehm *et al.* [Palo Verde Collaboration], Phys. Rev. D **64** (2001) 112001.
- [11] M. Mezzetto, T. Schwetz, J. Phys. **G37** (2010) 103001.
- [12] K. Nakamura, S. T. Petcov “Neutrino mass, mixing, and oscillations” in K. Nakamura *et al.* (Particle Data Group), J. Phys. G **37**, 075021 (2010).
- [13] P.F. Harrison, D.H. Perkins and W.G. Scott, Phys. Lett. B **530** (2002) 167.
- [14] H. Harari, Phys. Lett. **B216** (1989) 413.
- [15] J. R. Ellis, J. L. Lopez, D. V. Nanopoulos, Phys. Lett. **B292** (1992) 189.
- [16] P. Minkowski, Phys. Lett. B **67** (1977) 421; T. Yanagida, in Proceedings of the Workshop on the Unified Theory and the Baryon Number in the Universe (O. Sawada and A. Sugamoto, eds.), KEK, Tsukuba, Japan, 1979, p. 95; M. Gell-Mann, P. Ramond, and R. Slansky, in Supergravity (P. van Nieuwenhuizen and D. Z. Freedman, eds.), North Holland, Amsterdam, 1979, p. 315; S. L. Glashow, in Proceedings of the 1979 Cargese Summer Institute on Quarks and Leptons, Plenum Press, New York, 1980, p. 687; R. N. Mohapatra and G. Senjanovic, Phys. Rev. Lett. **44** (1980) 912.
- [17] J. Altegoer *et al.* [NOMAD Collaboration], Nucl. Instrum. Meth. **A404** (1998) 96.
- [18] E. Eskut *et al.* [CHORUS Collaboration], Nucl. Instrum. Meth. **A401** (1997) 7.
- [19] E. Heijne. CERN Yellow Report 83-06 (1983); G. Acquistapace *et al.* CERN Preprint CERN-ECP/95-14 (1995); L. Casagrande *et al.* CERN Yellow Report 96-06 (1996).
- [20] N. Abgrall *et al.*, “Time Projection Chambers for the T2K Near Detectors,” arXiv:1012.0865 [physics.ins-det].
- [21] N. Ushida *et al.* [FERMILAB E531 Collaboration], Phys. Rev. Lett. **57** (1986) 2897.
- [22] K. S. McFarland, D. Naples, C. G. Arroyo, P. S. Auchincloss, P. de Barbaro, A. O. Bazarko, R. H. Bernstein, A. Bodek *et al.*, Phys. Rev. Lett. **75** (1995) 3993.
- [23] S. Aoki, E. Barbuto, C. Bozza, J. P. Fabre, W. Flegel, G. Grella, M. Guler, T. Hara *et al.*, Nucl. Instrum. Meth. **A447** (2000) 361.
- [24] P. Annis *et al.* [CHORUS Collaboration], Nucl. Instrum. Meth. A **412** (1998) 19.
- [25] F. Bergsma *et al.*, Nucl. Instrum. Meth. A **357** (1995) 243.
- [26] J. W. E. Uiterwijk *et al.*, Nucl. Instrum. Meth. A **409** (1998) 682.
- [27] E. Di Capua *et al.*, Nucl. Instrum. Meth. A **378** (1996) 221.
- [28] E. Eskut *et al.* [CHORUS Collaboration], Nucl. Phys. **B793** (2008) 326.
- [29] P. Astier *et al.* [NOMAD Collaboration], Nucl. Phys. **B611** (2001) 3.

- [30] Y. Fukuda *et al.* [Super-Kamiokande Coll.], Phys. Rev. Lett. **81** (1998) 1562.
- [31] Y. Ashie *et al.* [Super-Kamiokande Coll.], Phys. Rev. Lett. **93** (2004) 101801; M. Ambrosio *et al.* [MACRO Coll.], Phys. Lett. B **517** (2001) 59; M. Sanchez *et al.* [Soudan 2 Coll.], Phys. Rev. D **68** (2003) 113004.
- [32] S. Fukuda *et al.* [Super-Kamiokande Collaboration], Phys. Rev. Lett. **85** (2000) 3999; P. Adamson *et al.* [MINOS Collaboration], Phys. Rev. Lett. **101** (2008) 221804.
- [33] Y. Ashie *et al.* [Super-Kamiokande Collaboration], Phys. Rev. Lett. **93** (2004) 101801.
- [34] L. Pasquali, M. H. Reno, Phys. Rev. **D59** (1999) 093003.
- [35] K. Abe *et al.* [Super-Kamiokande Collaboration], Phys. Rev. Lett. **97** (2006) 171801.
- [36] C. Rubbia, “The liquid Argon Time Projection Chamber: a new concept for Neutrino Detector, CERN-EP/77-08.
- [37] S. Amerio *et al.* [ICARUS Collaboration], Nucl. Instrum. Meth. A **527** (2004) 329; A. Menegolli [ICARUS Collaboration], J. Phys. Conf. Ser. **203** (2010) 012107.
- [38] J. Conrad, A. de Gouvea, S. Shalgar *et al.*, Phys. Rev. **D82** (2010) 093012.
- [39] T. Schwetz, M. A. Tortola, J. W. F. Valle, New J. Phys. **10** (2008) 113011.
- [40] F. Ardellier *et al.* [Double Chooz Collaboration], arXiv:hep-ex/0606025.
- [41] S. B. Kim [RENO Collaboration], AIP Conf. Proc. **981** (2008) 205 [J. Phys. Conf. Ser. **120** (2008) 052025].
- [42] Y. Itow *et al.* [T2K Collaboration], arXiv:hep-ex/0106019.
- [43] X. Guo *et al.* [Daya-Bay Collaboration], arXiv:hep-ex/0701029.
- [44] D. S. Ayres *et al.* [NOvA Collaboration], arXiv:hep-ex/0503053.
See also <http://www-nova.fnal.gov>.
- [45] Y. Hayato, Nucl. Phys. B (Proc. Suppl.) **112** (2002) 171; K. Hagiwara *et al.*, Nucl. Phys. B **668** (2003) 364.
- [46] Y. Itow [Super-Kamiokande Collaboration], J. Phys. Conf. Ser. **120** (2008) 052037.
- [47] T. Kato, Ph.D. Thesis, Stony Brook University, May 2007 (available at <http://www-sk.icrr.u-tokyo.ac.jp/sk/pub/index.html>).
- [48] R. Wendell, Talk at 11th International Workshop on Next generation Nucleon Decay and Neutrino Detectors, December 13-16, 2010, Toyama, Japan.
- [49] Ed. K. Elsener, “The CERN Neutrino beam to Gran Sasso (Conceptual Technical Design)”, CERN 98-02, INFN/AE-98/05; R. Bailey *et al.*, “The CERN Neutrino beam to Gran Sasso (NGS)” (Addendum to report CERN 98-02, INFN/AE-98/05), CERN-SL/99-034(DI), INFN/AE-99/05.
- [50] A. Ereditato, K. Niwa and P. Strolin, The emulsion technique for short, medium and long baseline $\nu_\mu \rightarrow \nu_\tau$ oscillation experiments, 423, INFN-AE-97-06, DAPNU-97-07; OPERA collaboration, H. Shibuya *et al.*, Letter of intent: the OPERA emulsion detector for a long-baseline neutrino-oscillation experiment, CERN-SPSC-97-24, LNGS-LOI-8-97.
- [51] M. Guler *et al.* [OPERA collaboration], An appearance experiment to search for $\nu_\mu \rightarrow \nu_\tau$ oscillations in the CNGS beam: experimental proposal, CERN-SPSC-2000-028, LNGS P25/2000
- [52] M. Guler *et al.*, [OPERA collaboration] Status Report on the OPERA experiment, CERN/SPSC 2001-025, LNGS-EXP 30/2001 add. 1/01
- [53] R. Acquafredda *et al.* [OPERA collaboration], New J. Phys. **8** (2006) 303; N. Agafonova *et al.* [OPERA collaboration], JINST **4** (2009) P06020.
- [54] K. Kodama *et al.* [DONUT Collaboration], Phys. Lett. **B504** (2001) 218; K. Kodama *et al.* [DONuT Collaboration], Phys. Rev. **D78** (2008) 052002.
- [55] R. Acquafredda *et al.* [OPERA collaboration], JINST **4** (2009) P04018.
- [56] N. Armenise *et al.*, Nucl. Instrum. Meth. **A551** (2005) 261; M. De Serio *et al.*, Nucl. Instrum. Meth. **A554** (2005) 247; L. Arrabito *et al.*, Nucl. Instrum. Meth. **A568** (2006) 578.
- [57] K. Morishima and T. Nakano, JINST (2010) 5 P04011.
- [58] A. Anokhina *et al.* [OPERA collaboration], JINST **3** (2008) P07002; A. Anokhina *et al.* [OPERA collaboration], JINST **3** (2008) P07005; T. Adam *et al.* [OPERA collaboration], Nucl. Instrum. Meth. **A577** (2007) 523; T. Nakamura *et al.* [OPERA collaboration], Nucl. Instrum. Meth.

- A556** (2006) 80.
- [59] N. Agafonova *et al.* [OPERA Collaboration], Phys. Lett. **B691** (2010) 138.
- [60] S. Geer, Phys. Rev. D **57** (1998) 6989 [Erratum-ibid. D **59** (1999) 039903]; A. De Rujula, M. B. Gavela and P. Hernandez, Nucl. Phys. B **547** (1999) 21.
- [61] F. Terranova, A. Marotta, P. Migliozzi and M. Spinetti, Eur. Phys. J. C **38** (2004) 69; S. K. Agarwalla, A. Raychaudhuri and A. Samanta, Phys. Lett. B **629** (2005) 33; S. K. Agarwalla, S. Choubey, A. Raychaudhuri *et al.*, JHEP **0806** (2008) 090; S. K. Agarwalla, S. Choubey, A. Raychaudhuri, Nucl. Phys. **B805** (2008) 305.
- [62] A. Cervera-Villanueva, “ISS/IDS detector study,” AIP Conf. Proc. **981** (2008) 51.
- [63] A. Bandyopadhyay *et al.* [ISS Physics Working Group], arXiv:0710.4947 [hep-ph].
- [64] J. S. Berg *et al.* [ISS Accelerator Working Group], JINST **4** (2009) P07001.
- [65] J. Burguet-Castell, M. B. Gavela, J. J. Gomez-Cadenas, P. Hernandez and O. Mena, Nucl. Phys. B **608** (2001) 301; H. Minakata and H. Nunokawa, JHEP **0110** (2001) 001; V. Barger, D. Marfatia and K. Whisnant, Phys. Rev. D **65** (2002) 073023.
- [66] P. Zucchelli, Phys. Lett. B **532** (2002) 166; M. Lindroos and M. Mezzetto, “Artificial Neutrino Beams: Beta Beams”, Imperial College Press, Aug. 2009.
- [67] A. Donini, D. Meloni and P. Migliozzi, Nucl. Phys. B **646** (2002) 321.
- [68] A. Cervera *et al.*, Nucl. Phys. **B579** (2000) 17, erratum ibid. Nucl. Phys. **B593** (2001) 731; M. Freund, Phys. Rev. **D64** (2001) 053003; E. K. Akhmedov, R. Johansson, M. Lindner *et al.*, JHEP **0404** (2004) 078.
- [69] D. Autiero *et al.*, Eur. Phys. J. **C33** (2004) 243.
- [70] A. Cervera, A. Laing, J. Martin-Albo *et al.*, Nucl. Instrum. Meth. **A624** (2010) 601.
- [71] S. K. Agarwalla, P. Huber, J. Tang *et al.*, JHEP **1101** (2011) 120.
- [72] D. Indumathi, N. Sinha, Phys. Rev. **D80** (2009) 113012.
- [73] A. Donini, J. J. Gomez Cadenas, D. Meloni, arXiv:1005.2275 [hep-ph].
- [74] L. Wolfenstein, Phys. Rev. **D17** (1978) 2369; S. P. Mikheyev and A. Y. Smirnov, Sov. J. Nucl. Phys. **42** (1985) 913; S. P. Mikheyev and A. Y. Smirnov, Nuovo Cim. **C9** (1986) 17.
- [75] J. W. F. Valle, J. Phys. **G29** (2003) 1819.
- [76] M. Guzzo, P. C. de Holanda, M. Maltoni, H. Nunokawa, M. A. Tortola, J. W. F. Valle, Nucl. Phys. **B629** (2002) 479.
- [77] A. A. Aguilar-Arevalo *et al.* [MiniBooNE Collaboration], Phys. Rev. Lett. **102** (2009) 101802.
- [78] A. A. Aguilar-Arevalo *et al.* [MiniBooNE Collaboration], Phys. Rev. Lett. **105** (2010) 181801.
- [79] M. C. Gonzalez-Garcia, M. Maltoni, J. Salvado, JHEP **1105** (2011) 075.
- [80] A. Palazzo, Phys. Rev. **D83** (2011) 101701.
- [81] E. Akhmedov, T. Schwetz, JHEP **1010** (2010) 115.
- [82] S. Davidson, C. Pena-Garay, N. Rius, A. Santamaria, JHEP **0303** (2003) 011.
- [83] S. Antusch, C. Biggio, E. Fernandez-Martinez, M. B. Gavela, J. Lopez-Pavon, JHEP **0610** (2006) 084.
- [84] R. Alonso, S. Antusch, M. Blennow, P. Coloma, A. de Gouvea, E. Fernandez-Martinez, B. Gavela, C. Gonzalez-Garcia *et al.*, “Summary report of MINSIS workshop in Madrid,” arXiv:1009.0476 [hep-ph].
- [85] M. Maltoni, J. Phys. Conf. Ser. **136** (2008) 022024.
- [86] M. Blennow, D. Meloni, T. Ohlsson, F. Terranova, M. Westerberg, Eur. Phys. J. **C56** (2008) 529.
- [87] A. Esteban-Pretel, J. W. F. Valle, P. Huber, Phys. Lett. **B668** (2008) 197.
- [88] J. Kopp, T. Ota, W. Winter, Phys. Rev. **D78** (2008) 053007.
- [89] A. Aguilar *et al.* [LSND Collaboration], Phys. Rev. **D64** (2001) 112007.
- [90] J. Kopp, M. Maltoni, T. Schwetz, “Are there sterile neutrinos at the eV scale?,” arXiv:1103.4570 [hep-ph].
- [91] A. Donini, M. Maltoni, D. Meloni, P. Migliozzi, F. Terranova, JHEP **0712** (2007) 013.
- [92] A. Donini, K. Fuki, J. Lopez-Pavon, D. Meloni, O. Yasuda, JHEP **0908** (2009) 041.
- [93] D. Meloni, J. Tang, W. Winter, Phys. Rev. **D82** (2010) 093008.

- [94] T. Abe *et al.* [ISS Detector Working Group Collaboration], JINST **4** (2009) T05001.
- [95] C. Fukushima, M. Kimura, S. Ogawa, H. Shibuya, G. Takahashi, K. Kodama, T. Hara, S. Mikado, Nucl. Instrum. Meth. **A592** (2008) 56.